Journal of Materials Science and Engineering with Advanced Technology
Volume 6, Number 1-2, 2012, Pages 71-115

QUANTIFICATION OF CORROSION RATE UNDER SALT FOG CORROSION TEST AND PITTING CORROSION TEST ON AZ61A MAGNESIUM ALLOY WELDS

A. DHANAPAL[1], S. RAJENDRA BOOPATHY[2], V. BALASUBRAMANIAN[3] and A. R. THOHEER ZAMAN[1]

[1]Department of Mechanical Engineering
Sri Ramanujar Engineering College
Vandalur, Chennai-600048
Tamil Nadu
India
e-mail: sridhanapal2010@gmail.com

[2]Department of Mechanical Engineering
College of Engineering
Anna University
Chennai-600025
Tamil Nadu
India

[3]Center for Materials Joining and Research (CEMAJOR)
Department of Manufacturing Engineering
Annamalai University
Annamalai Nagar
Chidambaram-608002
Tamil Nadu
India

Keywords and phrases: magnesium, weight loss, SEM, x-ray diffraction, welding, pitting corrosion.

Received November 5, 2012; Revised November 26, 2012

Abstract

Magnesium alloy plates of 6mm thick of AZ61A grade were butt welded using a solid state, autogenous, friction stir welding process. The joints were exposed under salt fog and electrochemical environments to characterize the corrosion rates of the FSW welds with the influence of pH, chloride ion concentration and the corrosion time in service applications to ensure such research is as effective as possible. The salt fog and pitting corrosion was quantified with different corrosion parameters. The corrosion rates were higher in salt fog conditions than the electrochemical performance of FSW welds.

1. Introduction

Magnesium alloys have received extensive recognition due to their excellent physical properties, including light weight, high strength/ weight ratio, high thermal conductivity, and good electromagnetic shielding characteristics, thus becomes a promising candidate to replace steel and aluminum alloys in many structural, mechanical, and practical applications due to their attractive mechanical and metallurgical properties [16, 29]. The joining of magnesium components made from this alloy, is however still limited. Unfortunately, conventional fusion welding of magnesium alloys often produces porosity, hot cracks etc., in the welded joint. This deteriorates both the mechanical properties as well as corrosion resistance [17, 28]. Hence, it will be of extreme benefit if a solid state joining process, i.e., one which avoids bulk melting of the base materials, hot cracking and porosity, can be developed and implemented for the joining of magnesium alloys.

FSW is a solid state welding process without emission of ration or dangerous fumes and it avoids the formation of solidification defects like hot cracking and porosity. Moreover, it is an environmental cleaner welding process. In addition, it significantly improved the weld properties and had been extensively applied in joining of magnesium alloys and aluminum alloys [27]. The application of Mg alloy in structural members is still limited due to its conventional fusion welding resulting in many solidifications related problems, such as hot cracking, porosity, alloy at segregation, and partial melting zone. To overcome from the above said problems, FSW process had been used, which is a solid state autogeneous process and hence there are no melting and solidification defects.

However, the corrosion resistances of the Mg-based alloys are generally inadequate due to the low standard electrochemical potential $-2.37V_{SHE}$ (standard hydrogen electrode) [31] and this limits the range of applications for Mg and its alloys. Therefore, the study of corrosion behaviour of magnesium alloys in active media, especially those containing aggressive ions, is crucial to the understanding the corrosion mechanisms, and hence, to improving the corrosion resistance under various service conditions. The scope of this paper is to examine the recent literature to further examine the electrochemical measurement hypothesis for Mg alloys and its weldments. Also, it aims to facilitate research directed at Mg alloy development and at understanding corrosion of Mg alloy and its friction stir welds in service applications to ensure such research is as effective as possible, where the pH value, chloride ion concentration, and corrosion time as the corrosion parameters. For research that uses polarization tests to elucidate corrosion of Mg alloy associated with service, it is strongly recommended that the research should be complemented by the use of two of the three other simple measurement methods: (i) weight loss rate; (ii) hydrogen evolution rate; and (iii) rate of Mg^{2+} leaving the metal surface. There is much better insight for little additional effort [19]. Other methods to rapidly determine the corrosion rates are (1) measuring the amount of hydrogen gas evolved [15] and (2) measuring the pH of the salt solution [26] with time. In both methods, however, the hydrogen concentration of the salt solution decreases significantly with time, causing precipitation of $Mg(OH)_2$ on the surface of the samples. This affects the intrinsic corrosion rate. Therefore, both methods are not capable of measuring the effect of a small change in composition on the intrinsic rate of magnesium corrosion. A novel and probably the only chemical means to rapidly determine the intrinsic rate of magnesium corrosion is to measure the amount of hydrogen ion. Thus, the salt fog corrosion tests were performed without recycling the solution, for the reason to obtain better intrinsic rate of corrosion.

This research focused on comparing salt spray corrosion with potentiodynamic polarization tests, which are the two main techniques for the corrosion studies in an effort to expose the magnesium alloy and its welds to environments similar to those environments experienced for service applications. From the literature review, it was understood that most of the published information on corrosion behaviour of Mg alloys were focused on general corrosion and pitting corrosion of unwelded base alloys. Very few investigations have been conducted so far on corrosion behaviour of FSW joints of Mg alloys. The aim of this research is to investigate the occurrence of salt spray corrosion in FSW welds and the electrochemical behaviour of friction stir welded AZ61A magnesium alloy for service applications with the propitious to study the effect of pH value, chloride ion concentration, and corrosion time on corrosion rate of AZ61A magnesium alloy welds.

2. Experimental Procedure

2.1. Test materials

The material used in this study was AZ61A magnesium alloy in the form of extruded condition and supplied in plates of 6mm thickness. The chemical composition and mechanical properties of the base metal are presented in Tables 1(a) and 1(b). The optical micrograph of base metal is shown in Figure 1; it was observed that the microstructure of base metal contains coarse grains with $Al_{12}Mg_{17}$ intermetallic compounds.

Table 1. (a) Chemical composition (wt%) of AZ61A Mg alloy

Al	Zn	Mn	Mg
5.45	1.26	0.17	Balance

Table 1. (b) Mechanical properties of AZ61A Mg alloy

Yield Strength (MPa)	Ultimate Tensile Strength (MPa)	Elongation (%)	Vickers hardness at 0.05kg load (Hv)
176.49	271.68	8.40	56.3

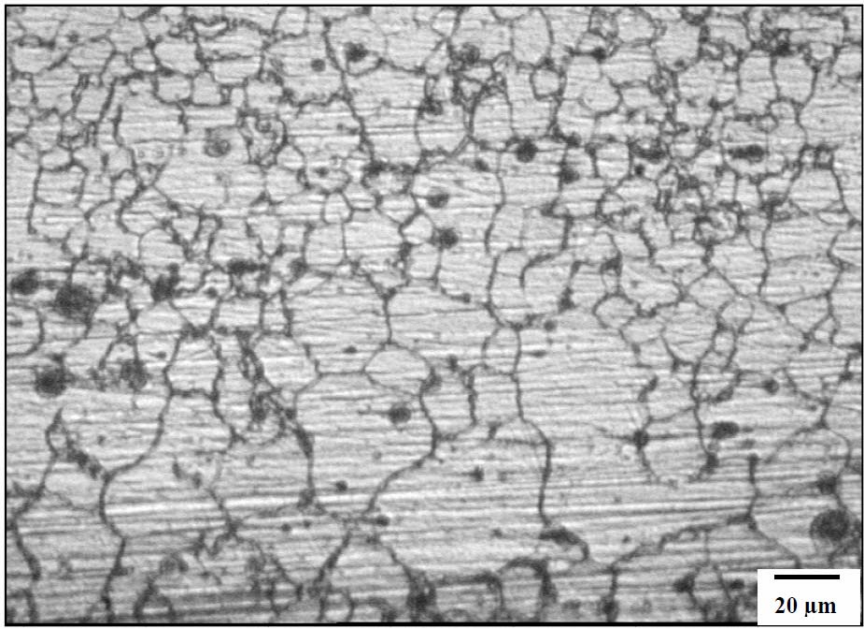

Figure 1. Optical micrograph of AZ61A base metal.

2.2. Fabricating the joints and preparing the specimens

The plate was cut to a required size (300mm × 150mm) by power hacksaw followed by milling. A square butt joint configuration was prepared to fabricate the joints. The initial joint configuration was obtained by securing the plates in position by using mechanical clamps. The direction of welding was normal to the extruded direction. Single pass welding procedure was followed to fabricate the joints. A non-consumable tool made of high carbon steel was used to fabricate joints. An indigenously designed and developed computer numerical controlled friction stir welding machine (22kW, 4000 RPM, 60kN) was used to fabricate joints. The FSW parameters were optimized by conducting trial runs and the welding conditions, which produced defect free joints were taken as optimized welding conditions. The optimized welding conditions used to fabricate the joints in this investigation are presented in Table 2. The specimens were ground with $500^{\#}$, $800^{\#}$, $1200^{\#}$, $1500^{\#}$ grit SiC

paper. Finally, it was cleaned with acetone and washed in distilled water, then dried by warm flowing air. The optical micrograph of the stir zone of the FSW joint of AZ61A magnesium alloy is shown in Figure 2; here, it reveals that the stir zone contains fine grains with significantly refined $Al_{12}Mg_{17}$ intermetallic compounds, which are not uniformly distributed in the magnesium matrix.

Table 2. Optimized welding conditions and process parameters used to fabricate the joints

Rotational speed (rpm)	Welding speed (mm/min)	Axial force (kN)	Tool shoulder diameter (mm)	Pin diameter (mm)	Pin length (mm)	Pin profile
1000	75	3	18	6	5	Left hand thread of 1mm pitch

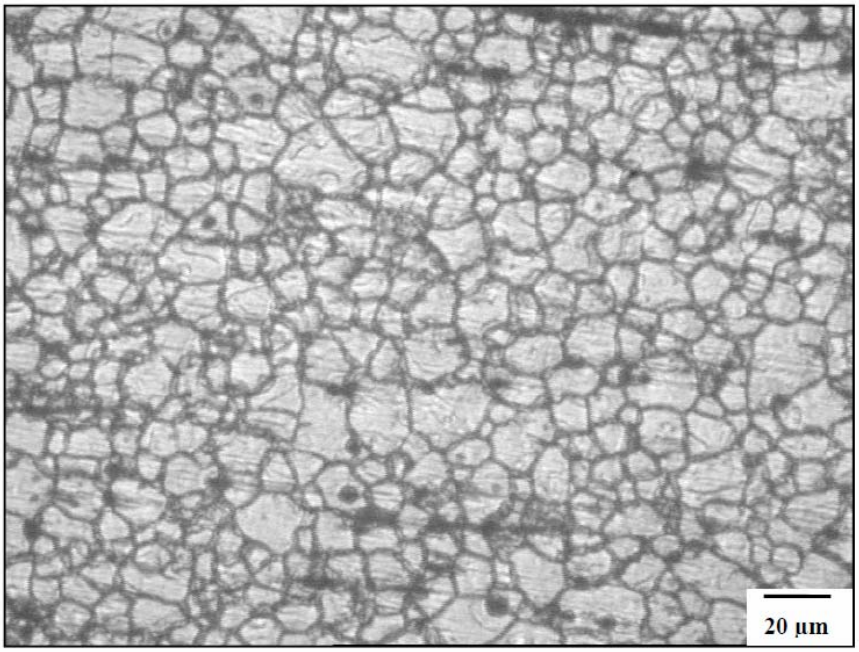

Figure 2. Optical micrograph of stir zone of FSW AZ61A Mg alloy.

2.3. Finding the limits of corrosion test parameters

From the literature [1, 23, 26], the predominant factors that have a greater influence on corrosion behaviour of AZ61A magnesium alloy are identified. They are: (i) pH value of the solution; (ii) exposure time; and (iii) chloride ion concentration. Large numbers of trial experiments were conducted to identify the feasible testing conditions using friction stir welded AZ61A magnesium alloy joints under novel test conditions. The following inferences are obtained:

(1) If the pH value of the solution was less than 3 -the change in chloride ion concentration did not considerably affect the corrosion potential during electrochemical measurements.

(2) If the pH value was in between 3 to 11 -there were inhibition of the corrosion process and stabilization of the protective layer.

(3) If the pH value was greater than 11 -blocking of further corrosion by the active centers of protective layer.

(4) If the chloride ion concentration was less than 0.2M -the visible corrosion did not occur in the experimental period.

(5) If the chloride ion concentration was in between 0.2M and 1M -there was a reasonable fluctuation in the corrosion rate.

(6) If the chloride ion concentration was greater than 1M - rise in corrosion rate slightly decreased a little.

(7) If the exposure time was less than an hour -the surface would be completely covered with thick and rough corrosion products.

(8) If the exposure time was in between 1 to 9 hours - the short term corrosion could be predicted.

(9) If the exposure time was greater than 9 hours -the enhancement of corrosion film, causing a strike against corrosion, which makes difficult to identify the corrosion.

2.4. Experimental design matrix

Owing to a wide range of factors, the use of three factors and central composite rotatable design matrix was chosen to minimize number of experiments. The assay conditions for the reaction parameters were taken at zero level (center point) and one level $(+1)$ and (1). The design was extended up to a $\pm\alpha$ (axial point) of 1.68. The center values for variables were carried out at least six times for the estimation of error and single runs for each of the other combinations; twenty runs were done in a totally random order. The design would consist of the eight corner points of the 2^3 cube, the six star points, and m center points [6]. The star points would have $a = 8\text{^}(1/4) = 1.682$.

Design matrix consisting of 20 sets of coded conditions (comprising a full replication three factorial of 8 points, six corner points, and six center points) was chosen in this investigation. Table 3 represents the ranges of factors considered, and Table 4 shows the 20 sets of coded and actual values used to conduct the experiments. For the convenience of recording and processing experimental data, the upper and lower levels of the factors were coded here as $+1.682$ and -1.682, respectively. The coded values of any intermediate value could be calculated by using following relationship:

$$X_i = \frac{1.682 \times \{2X - [(X_{\max} - X_{\min})]\}}{X_{\max} - X_{\min}}, \quad (1)$$

where X_i is the required coded value of a variable X and X is any value of the variable from $X_{\min}$ to $X_{\max}$;

$X_{\min}$ is the lower level of the variable;

$X_{\max}$ is the upper level of the variable.

Table 3. Important factors and their levels

Sl. No.	Factor	Unit	Notation	Levels				
				– 1.682	– 1	0	+ 1	+ 1.682
1	pH value		P	3	4.62	7	9.38	11
2	Exposure time	Hours (h)	t	1	2.62	5	7.38	9
3	Cl^- concentration	Mole(M)	C	0.2	0.36	0.6	0.84	1

Table 4. Design matrix and experimental results

EX. No.	Actual values			Weight loss,w (mg/ testing hours)	Hydrogen evolution rate, V_H (ml/testing hours)	Corrosion Current density, i_{corr} (mA/cm^2)	Corrosion rate (mm/yr)		
	pH	Time t (hour)	Conc. C (M)				Salt for corrosion test (R_w)	Hydrogen evolution (R_H)	Pitting corrosion test (R_i)
1	4.62	2.62	0.36	0.0182	0.0171	0.2892	14.62 (0.213)	13.80 (0.054)	6.608 (0.188)
2	9.38	2.62	0.36	0.0133	0.0123	0.2016	10.23 (0.126)	9.44 (0.145)	4.606 (0.125)
3	4.62	7.38	0.36	0.0146	0.0136	0.1840	11.89 (0.257)	11.07 (0.212)	4.204 (0.325)
4	9.38	7.38	0.36	0.0311	0.0286	0.1271	8.99 (0.179)	8.26 (0.214)	2.904 (0.256)
5	4.62	2.62	0.84	0.0194	0.0179	0.4032	15.82 (0.176)	14.58 (0.051)	9.213 (0.233)
6	9.38	2.62	0.84	0.0141	0.0130	0.2454	11.31 (0.124)	10.48 (0.158)	5.607 (0.249)
7	4.62	7.38	0.84	0.0447	0.0410	0.3594	12.92 (0.16)	11.85 (0.186)	8.212 (0.143)
8	9.38	7.38	0.84	0.0372	0.0342	0.2936	10.75 (0.235)	9.88 (0.147)	6.708 (0.125)
9	3	5	0.60	0.0422	0.0390	0.2832	17.96 (0.335)	16.60 (0.258)	8.471 (0.203)
10	11	5	0.60	0.0161	0.0150	0.2016	8.88 (0.138)	7.39 (0.122)	4.606 (0.050)
11	7	1	0.60	0.0052	0.0048	0.3717	11.23 (0.109)	10.33 (0.287)	8.208 (0.355)
12	7	9	0.60	0.0312	0.0290	0.1885	8.51 (0.211)	6.87 (0.114)	4.307 (0.022)
13	7	5	0.20	0.0179	0.0165	0.1972	11.66 (0.157)	7.06 (0.365)	4.506 (0.016)
14	7	5	1	0.0288	0.0265	0.3900	15.28 (0.118)	11.29 (0.210)	8.911 (0.227)
15	7	5	0.60	0.0232	0.0212	0.2630	9.89 (0.186)	9.12 (0.129)	6.00 (0.207)
16	7	5	0.60	0.0232	0.0212	0.2630	9.89 (0.186)	9.12 (0.129)	6.00 (0.207)
17	7	5	0.60	0.0232	0.0212	0.2630	9.89(0.186)	9.12 (0.129)	6.00 (0.207)
18	7	5	0.60	0.0232	0.0212	0.2630	9.89(0.186)	9.12 (0.129)	6.00 (0.207)
19	7	5	0.60	0.0232	0.0212	0.2630	9.89(0.186)	9.12 (0.129)	6.00 (0.207)
20	7	5	0.60	0.0232	0.0212	0.2630	9.89(0.186)	9.12 (0.129)	6.00 (0.207)

Owing to a wide range of factors, the use of three factors and central composite rotatable design matrix was chosen to minimize the number of experiments. Design matrix consisting 20 sets of coded conditions (comprising a full replication three factorial of 8 points, six corner points, and six center points) was chosen in this investigation.

*The values presented in bracket are the standard deviation among the triplicate tests results. The tests results were carried out in triplicate to ensure the reproducibility of the results.

2.5. Salt fog corrosion test

Solution of NaCl with concentrations of 0.2M, 0.36M, 0.6M, 0.84M, and 1M were prepared. The pH value of the solution was used here as, pH 3, pH 4.62, pH 7, pH 9.38, and pH 11. In order to obtain a calibrated and desired pH, adding concentrated HCl and NaOH was enhanced for accuracy. The pH value was measured using a digital pH meter. The test method consists of exposing the specimens in a salt spray chamber (model: Salt Spray Cabinet, Make: SR Lab Instruments, INDIA, Control system: PID type, Fog collection: 0.5 to 3ml per hour) as per ASTM B 117 standards and evaluating the corrosion tested specimen with the method as per ASTM G1-03. Basically, the salt spray test procedure involves the spraying of a salt solution onto the samples being tested. This was done inside a temperature controlled chamber. The glass racks were contained in the salt fog chamber. The samples under test were inserted into the chamber, following which the salt-containing solution was sprayed as a very fine fog mist over the samples. NaCl in tapped water was pumped from a reservoir to spray nozzles. The solution was mixed with humidified compressed air at the nozzle and this compressed air, atomized the NaCl solution into a fog at the nozzle. Heaters were maintained at 35^{o}C cabinet temperature. Within the chamber, the samples were rotated frequently so that all samples were exposed uniformly to the salt spray mist. Since the spray was continuous, the samples were continuously wet, and therefore, uniformly subjected to corrosion.

2.6. Pitting corrosion test

The potentiodynamic polarizations measurements were carried out in corrosion test cell containing 500ml solution. The corrosion process parameters were chosen as same as in the salt spray corrosion tests,

which includes the pH value, the chloride ion concentration, and the exposure time. Corrosion testing carried out as per ASTM G5. An electrochemical polarizations experiment was carried out by using a potentiostat (model: GILL AC, Make: ACM Instruments, UK, Compliance voltage: ±15V, Operational temperature: – 5ºC to 72ºC). The electrochemical cell consists of friction stir welds of AZ61A magnesium alloy as the working electrode, a saturated calomel reference electrode, and a platinum counter electrode. The electrodes for this purpose were prepared by connecting a wire to one side of the sample that was covered with cold setting resin. Other side of the specimen, with an area of $1cm^2$, was exposed to NaCl solution for different exposure times. Short-term tests have provided corrosion rates for Mg alloys that do not agree with long term tests. But, in case of magnesium alloys, it corrodes aggressively with faster rates. Thus short term tests were enhanced. Moreoften, the corrosion rate Mg evaluated from Tafel plots has pertained to conditions soon after specimen immersion for stability and these corrosion rates have not related to steady state corrosion. The specimens were exposed and a polarizations scan was carried out towards more noble values at a rate 18mV/min. The scan scope was set from – 2000mV to 0mV vs. OCP. All electrochemical tests were conducted in triplicates in order to ensure the reproducibility of results. The corrosion potential was developed and observed from the open circuit potential. All potentials referred in the study are quoted with respect to the SCE. The corrosion current density (i_{corr}) was estimated by linear fit and the polarization curves were used to explore the relationship, if any between the electrochemical measurements of the corrosion rate, based on the corrosion current at the free corrosion potential, and direct measurements using weight loss and evaluated from the hydrogen evolved. The corrosion current at the free corrosion potential was evaluated by Tafel plots of the cathodic branch of the polarization curve. The cathodic curves were all linear; a slope was used similar to all curves between the cathodic and anodic curves.

2.7. Corrosion rate measurement

The simplest and most fundamental measurement of the corrosion rate is the metal weight loss rate, **w** (mg/testing hours) derived as per ASTM G-31. This can be converted to an average corrosion rate (mm/yr) using [3, 5, 7, 12].

$$\text{Corrosion rate (weight loss measurements) } R_w = \frac{8.76 \times 10^4 \times w}{A \times \rho \times t} \text{ mm / yr,} \quad (2)$$

where

w = weight loss in milligrams.

A = surface area of the specimen in cm^2.

ρ = density of the material, $1.72 gm/cm^3$.

t = corrosion time in hours.

In the overall corrosion reaction of pure Mg, one molecule of hydrogen is evolved for each atom of corroded Mg. One mol (i.e., 24.31g) of Mg metal corrodes for each mol (i.e., 22.4L) of hydrogen gas produced. Therefore, the hydrogen evolution rate, $V_H (ml/cm^2/d)$, is related to the metallic weight loss rate, w using [21, 24, 33]

$$w = 1.085\, V_H \text{mm/yr.} \quad (4)$$

The corresponding corrosion rate, R_H, is evaluated by substituting Equation (4) into Equation (2) to give

$$R_H = 2.279\, V_H \text{mm/yr.} \quad (5)$$

For Mg corrosion, there is excellent agreement [21, 24, 34] between the corrosion rate measured by the weight loss rate and that evaluated from the hydrogen evolution rate. In the potentiodynamic polarization test for measuring the corrosion rate, the corrosion current density i_{corr} (mA/cm^2) is estimated from the polarization curve, and i_{corr} is related to the average corrosion rate using [21, 24, 32]

Corrosion rate (potentio-dynamic polarization measurements),

$$R_i = 22.85\, i_{corr} \text{mm/yr.} \quad (6)$$

From the literature review, it was observed that, why this electrochemical technique might not give reliable values for Mg corrosion. Nevertheless, the electrochemical technique of polarization test is widely used for the evaluation of the corrosion of Mg alloys, at least partly, because it is a quick and easy technique. Therefore, it is useful to review the literature on this technique for Mg alloys. It is useful to have quantitative measures of the quality of the corrosion rate evaluated by the potentiodynamic polarization technique.

2.8. Metallography

Micro structural examination of the corroded specimens was carried out using a light optical microscope (Union Opt. Co. Ltd., Japan; Model: VERSAMET-3) incorporated with an image analyzing software (Clemex-vision). The exposed specimen surface was prepared for the micro examination with minor polish. The corrosion test specimens were polished in disc polishing machine for scratch free surfaces. To determine the depth and diameter of the pit, the exposed specimens were cut in cross-sectional, the corrosion products were removed, then the specimens were covered with cold setting resin and the surface was observed at 200× magnification. The corrosion products were analyzed by SEM-EDAX and X-ray diffraction analysis.

3. Developing an Empirical Relationship

The response surface methodology (RSM) approach was adopted in this study because of its following advantages: (1) the ability to evaluate the effects of interactions between tested parameters; (2) the benefit of limiting the number of actual experiments to be carried out, in comparison to a classical approach for the same number of estimated parameters [10, 35]. In the present investigation, to correlate the potentiodynamic polarization tests parameters and the corrosion rate of AZ61A welds, a second order quadratic model was developed. The

response (corrosion rate of AZ61A welds) is a function of pH values (P), exposure time (T), and chloride ion concentration (C) and it could be expressed as:

$$\text{Corrosion rate} = f(P, T, C). \tag{8}$$

In order to study the combined effects of these parameters, experiments were conducted at different combinations using statistically designed experiments. The empirical relationship must include the main and interaction effects of all factors and hence the selected polynomials are expressed as follows:

$$Y = b_0 + \sum b_i x_i + \sum b_{ii} x_i^2 + \sum b_{ij} x_i x_j. \tag{9}$$

For three factors, the selected polynomial could be expressed as

$$\text{Corrosion Rate} = \{b_0 + b_1(P) + b_2(T) + b_3(C) + b_{11}(P^2) + b_{22}(T^2) + b_{33}(C^2) + b_{12}(PT) + b_{13}(PC) + b_{23}(TC)\}, \tag{10}$$

where b_0 is the average of responses (corrosion rate) and b_1, b_2, b_3 … b_{11}, b_{12}, b_{13} … b_{22}, b_{23}, b_{33}, are the coefficients that depend on their respective main and interaction factors, which are calculated by using the expression given below:

$$B_i = \sum (X_i, Y_i) / n, \tag{11}$$

where 'i' varies from 1 to n, in which X_i is the corresponding coded values of a factor; Y_i is the corresponding response output values (corrosion rate) obtained from the experiment; and 'n' is the total number of combination considered. All the coefficients were obtained applying central composite rotatable design matrix including the Design Expert statistical software package. After determining the significant coefficients (at 95% confidence level), the final relationship was developed including only these coefficients. The final empirical relationship obtained by the above procedure to estimate the corrosion rate of friction stir welds of AZ61A magnesium alloy is given below:

For salt fog environments:

$$\text{Corrosion Rate} = 9.48 - 1.89(P) - 0.88(T) + 0.82(C) + 1.60(P^2) + 1.27(C^2)\ \text{mm/yr.} \quad (12)$$

For potentiodynamic polarization environments:

$$\text{Corrosion Rate} = 0.56 - 0.085(P) - 0.052(T) + 0.014(C) + 0.035(PT) + 0.051(TC) + 0.042(C^2)\ \text{mm/yr.} \quad (13)$$

3.1. Checking the adequacy of the model for salt spray testing

The analysis of variance (ANOVA) technique was used to find the significant main and interaction factors. The results of second order response surface model fitting in the form of analysis of variance (ANOVA) are given in the Table 5. The determination coefficient (r^2) indicated the goodness of fit for the model. The Model F-value of 31.30 implies the model is significant. There is only a 0.01% chance that a "Model F-Value" this large could occur due to noise. Values of "Prob > F" less than 0.0500 indicates model terms are significant. In this case, P, T, C, P^2, C^2 are significant model terms. Values greater than 0.1000 indicate the model terms are not significant. If there are many insignificant model terms (not counting those required to support hierarchy), model reduction may improve the model. The "Lack of Fit F-value" of 1.69 implies the Lack of Fit is not significant relative to the pure error. There is a 28.93% chance that a "Lack of Fit F-value" this large could occur due to noise. Non-significant lack of fit is good. The "Pred R-Squared" of 0.8176 is in reasonable agreement with the "Adj R-Squared" of 0.9349. "Adeq Precision" measures the signal to noise ratio. P ratio greater than 4 is desirable. The ratio of 19.440 indicates an adequate signal. All of this indicated an excellent suitability of the regression model. Each of the observed values compared with the experimental values shown in the Figure 3. A regression equation

(Equation (12)) was derived using the software package, which in turn proposed to correlate the predicted values with the observed (experimental) values. Thus, a residual was formed. The residuals are nothing but, the difference between the experimental corrosion rate and predicted corrosion rate. The residual is pictorially shown in the Figure 3. The distance between the center line and the red dotted lines in the Figure 3 was called as residual. The distance found very limit, indicates the error is within the limit and the points are scattered closer to the center line.

Table 5. ANOVA test results for salt fog corrosion test

Source	Sum of squares	df	Mean square	F-value	p-value Prob>F	
Model	126.60	9	14.07	31.30	<0.0001	**significant**
P	49.03	1	49.03	109.11	<0.0001	
T	10.55	1	10.55	23.48	0.0007	
C	9.12	1	9.12	20.29	0.0011	
PT	1.83	1	1.83	4.08	0.0710	
PC	0.047	1	0.047	0.10	0.7543	
TC	0.033	1	0.033	0.072	0.7934	
P^2	37.07	1	37.07	82.48	<0.0001	
T^2	3.4×10^{-4}	1	3.4×10^{-4}	7.6×10^{-4}	0.9785	
C^2	23.17	1	23.17	51.55	<0.0001	
Residual	4.49	10	0.45			
Lack of Fit	2.82	5	0.53	1.69	0.2893	**Not significant**
Pure Error	1.67	5	0.33			
Cor Total	131.09	19				

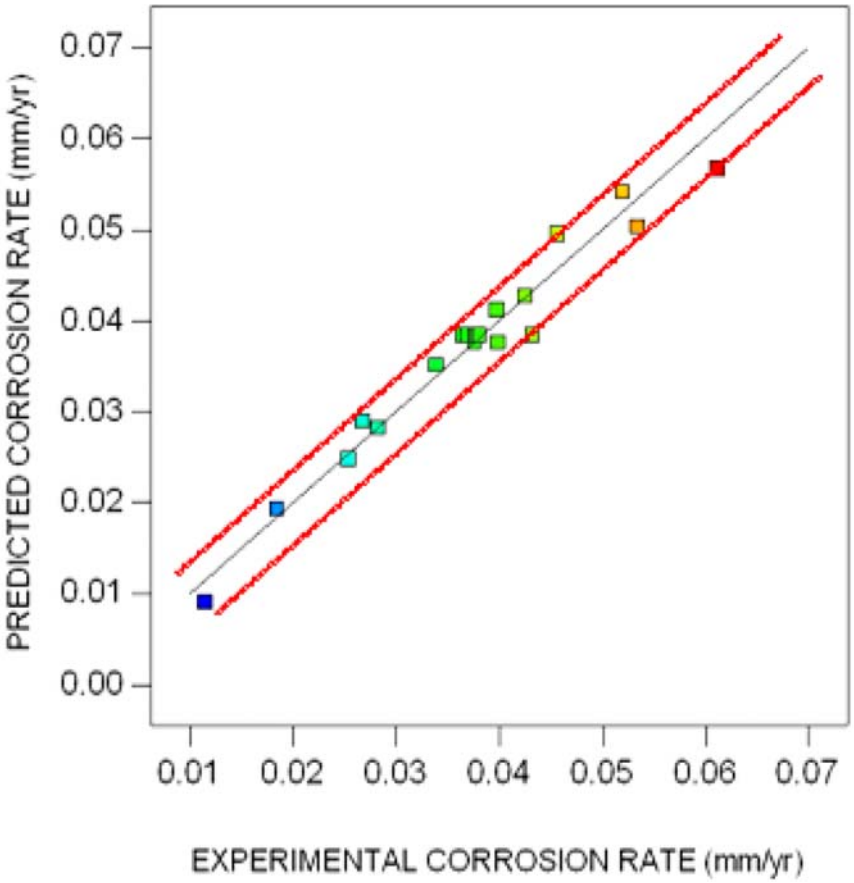

Figure 3. Correlation graph for response (salt spray corrosion test).

3.2. Checking the adequacy of the model for potentiodynamic polarization testing

It was thus conducted in this study in order to determine whether the above mentioned second order polynomial equation was significant fit with the experimental results. The results of the second order response surface model fitting as analysis of variance (ANOVA) are given in the Table 6. The determination coefficient (r^2) indicated the goodness of fit for the model. The Model F-value of 38.65 implies the model is significant. There is only a 0.01% chance that a "Model F-Value" this

large could occur due to noise. Values of "Prob > F" less than 0.0500 indicate model terms are significant. In this case, P, T, C, PT, TC, T^2 are significant model terms. Values greater than 0.1000 indicate the model terms were not significant. If there are many insignificant model terms (not counting those required to support hierarchy), model reduction may improve the model. The "Lack of Fit F-value" of 2.86 implies the Lack of Fit was not significant relative to the pure error. There was a 13.07% chance that a "Lack of Fit F-value" this large could occur due to noise. Non-significant lack of fit is good. The "Pred R-Squared" of 0.8256 is in reasonable agreement with the "Adj R-Squared" of 0.9469. "Adeq Precision" measures the signal to noise ratio. P ratios greater than 4 are desirable. The ratio of 22.605 indicates an adequate signal. All of this indicated an excellent suitability of the regression model. Each of the observed values compared with the experimental values shown in the Figure 4. A regression equation (Equation (13)) was also derived here to propose a correlation between the predicted and the observed (experimental) results forming a residual. The residuals are the difference between the experimental corrosion rate and predicted corrosion rate. The residual is pictorially shown in the Figure 4. It was observed that, the distance between the centre true line and the red dotted lines were found very limit, indicates the error is within the limit and the points are scattered closer to the center line.

Table 6. ANOVA test results for pitting corrosion test

Source	Sum of squares	df	Mean square	F-value	p-value Prob>F	
Model	0.46	9	0.051	38.65	< 0.0001	**significant**
P	0.098	1	0.098	74.98	< 0.0001	
T	0.037	1	0.037	28.34	0.0003	
C	0.26	1	0.26	196.08	< 0.0001	
PT	9.887×10^{-3}	1	9.887×10^{-3}	7.54	0.0206	
PC	4.652×10^{-3}	1	4.652×10^{-3}	3.55	0.0890	
TC	0.021	1	0.021	15.64	0.0027	
P^2	1.545×10^{-4}	1	1.545×10^{-4}	0.12	0.7385	
T^2	1.103×10^{-3}	1	1.103×10^{-3}	0.84	0.3807	
C^2	0.026	1	0.026	19.56	0.0013	
Residual	0.013	10	1.311×10^{-3}			
Lack of Fit	9.712×10^{-3}	5	1.942×10^{-3}	2.86	0.1370	**Not Significant**
Pure Error	3.400×10^{-3}	5	6.800×10^{-4}			
Cor Total	0.47	19				

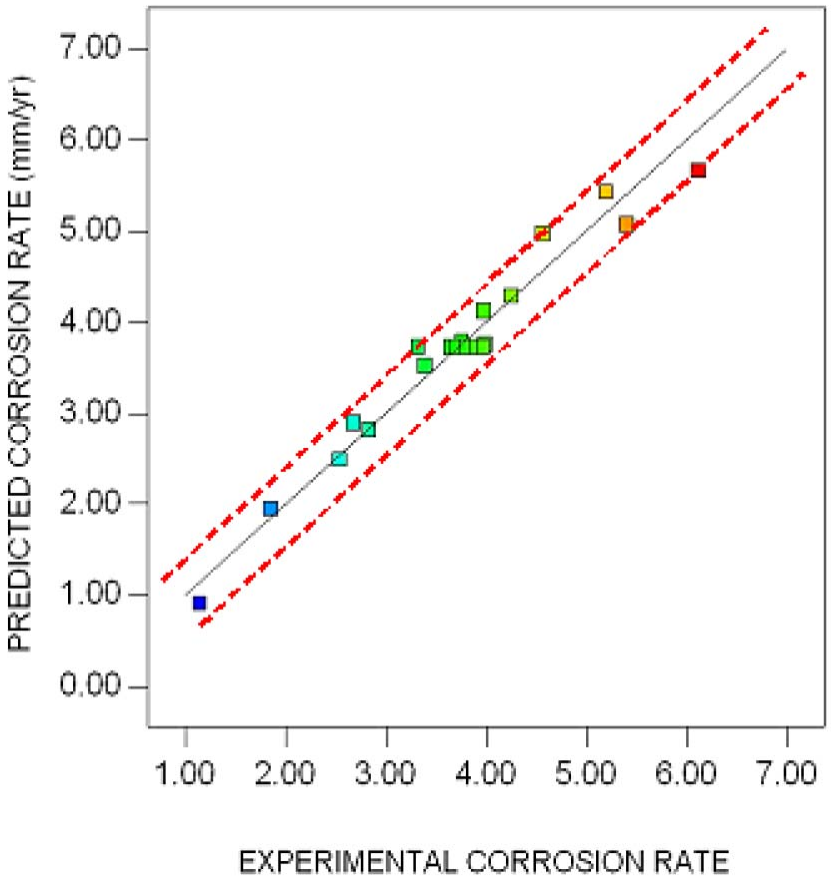

Figure 4. Correlation graph for response (pitting corrosion test).

4. Results and Discussion

Table 4 shows the weight loss during salt spray corrosion test (ΔW), hydrogen evolution rate (V_H), corrosion current density (i_{corr}) corrosion rate evaluated from weight loss method (CR_W), hydrogen evolution rate (CR_H), and potentiodynamic polarization test (CR_i) at different pH values, chloride ion concentration, and exposure time. This data shows that the corrosion rate evaluated from weight loss agrees within an error of ±10% with the corrosion rate independently measured from hydrogen evolution [19]. The weight loss data and hydrogen

evolution volumes were normalized to the surface area was shown in Figure 5. In order to quantify the results that, the corrosion rate evaluated from weight loss agrees within an error of ±10% with the corrosion rate independently measured from hydrogen evolution, a surface are plot was developed to prove better correlation between the weight loss and hydrogen evolution. The area plots reveal better constitutional agreement of error within 10%. The surface area of weight loss linearly agrees the surface area of the hydrogen volumes. Furthermore, statistically, it can be prove from the goodness of fit, called concordance correlation coefficient. It evaluates the degree to which the pair of observation (weight loss data and hydrogen volume data) falls on the 45° line through the origin [13]. It was observed from the kinetic plot shown in Figure 6. Also, the observations scattered a little and all points are fitted in a straight line. The concordance correlation coefficient measures a good agreement between the weight loss data and the hydrogen volume data by measuring the variation of their relationship from the 45° line through the origin. This coefficient also, measures how far each observation deviates from the line to the data [14].

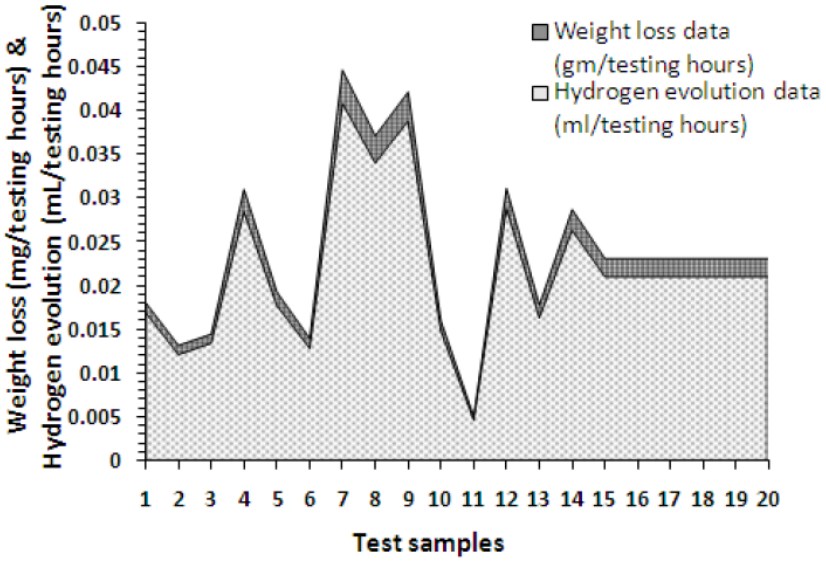

Figure 5. Normalized surface area plot to correlate the weight loss data and hydrogen volume data.

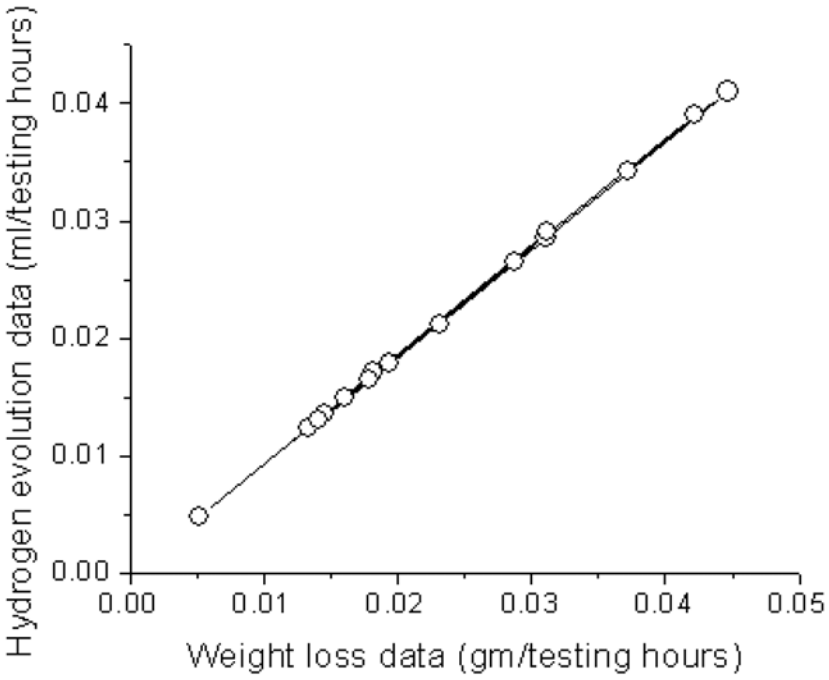

Figure 6. Kinetic plot to correlate the weight loss data and hydrogen volume data using concordance correlation coefficient.

The hydrogen evolution was measured and found that the corrosion initiated as localized corrosion at some sites on the surface and subsequently expanded over the whole surface. The hydrogen evolution, after an initiation time of several hours, increased linearly with exposure time. The advance of the corrosion over the surface of friction stir welds of AZ61A was slower, although the corrosion also initiated as localized corrosion. The hydrogen evolution, after an initiation time of several hours, increased with exposure time; the hydrogen evolution rate increased slightly with time. The incubation period was quiet long for pure Mg, there was essentially no incubation period for AZ61A magnesium alloy welds. Thereafter, there was an increase in hydrogen evolution with increasing exposure time. For most alloys, the rate of hydrogen evolution initially increased with increasing exposure time, which is attributed to corrosion occurring over increasing fractions of the surface as was observed.

A comparison of these values from Tafel plots with those calculated from the hydrogen evolution data indicated that (i) the corrosion rates were much higher when estimated from the hydrogen evolution rate and (ii) the corrosion rate estimated from the Tafel plots showed the same trends in influence of pH, chloride ion concentration, and corrosion time. The reason for the difference may be that different types of corrosion were measured. The corrosion rate from the Tafel plots may relate to the onset of corrosion, whereas the corrosion rate from the hydrogen evolution measurements relates to corrosion averaged over a considerable time period and includes corrosion some considerable time after corrosion onset, when the corrosion is well established. Tafel plots were used to evaluate i_{corr} and the corresponding corrosion rates have been designated.

Thus, the potentiodynamic polarization technique is essentially an instantaneous technique, which provides a measurement of the corrosion rate at a particular time over which the measurement was carried out. For Mg alloys, the corrosion rate can also be evaluated from the evolved hydrogen; this technique allows both an instantaneous measurement at any particular time during the exposure as well providing integration over the whole exposure period. In contrast, the weight loss measurement evaluates the corrosion rate as an average value over the exposure period. This means that a rigorous evaluation of polarization tests requires good measurements of Tafel plots under conditions that provide a measurement that is comparable to a corrosion rate measured by weight loss.

On a note on microstructure, all second phases have the tendency to cause micro-acceleration of the corrosion of the alpha-Mg matrix [21, 24, 33, 34], so a multi-phase alloy has typically a corrosion rate greater than that of pure Mg. The second phase can provide a barrier effect if it is essentially continuous and has a lower corrosion rate than the alpha-Mg matrix; otherwise, there is the tendency for the corrosion rate to be accelerated, even for second phase particles as small [2]. It was observed that, Mg alloys like AZ61A, the corrosion is caused by the beta phase accelerating the corrosion of the adjacent Mg alpha phase. The acceleration of the overall corrosion rate can be by a factor of 10-20 [18].

4.1. Effect of pH on corrosion rate

Figure 7 shows the effect of pH on Tafel plots with different pH values of pH 3, pH 7, and pH 11 with 0.6M concentration of NaCl for 5 hours. It was observed that with the decrease in the pH values of the solutions, the anodic curve of the materials showed a shift to more negative potential. However, even though is not thermodynamically stable at low pH values, the dissolution kinetics may be slower and a surface film may be formed provided the dissolution kinetics are slower than the formation kinetics. It was observed that the corrosion rate usually increased with the decrease in the pH values of the solutions [20]. It is due to the dissolution of α-magnesium. The α-magnesium dissolute easily in acidic medium and in aqueous solutions, the corrosion proceeds by the reduction of water to produce magnesium hydroxide. This reduction process was mainly water reduction, thus forming a $Mg(OH)_2$ protective layer. Higher the pH values favours the formation of $Mg(OH)_2$, which protects the alloy from corrosion.

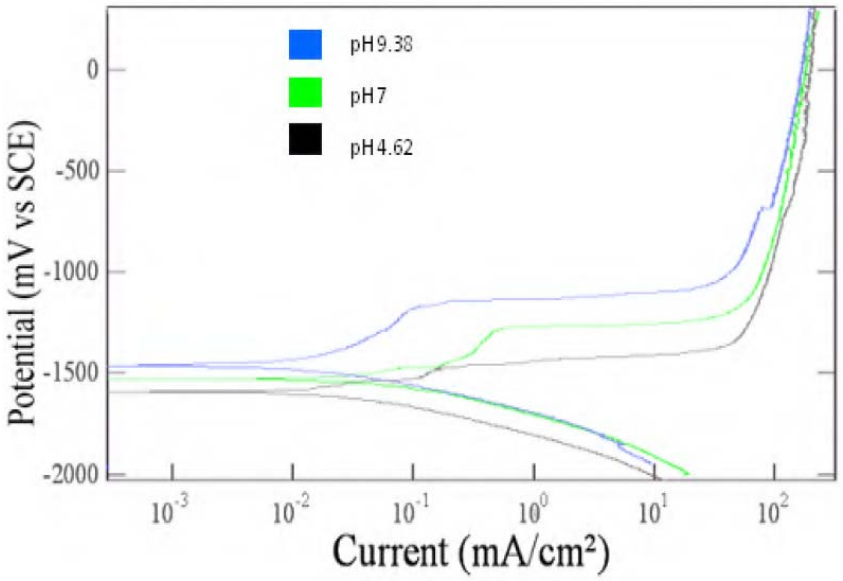

Figure 7. Effect of pH value on Tafel plots with different pH values of pH 3, pH 7, and pH 11 with 0.6M concentration of NaCl for 5 hours.

On comparing the corrosion rate of both the corrosion tested specimen with different pH values of pH 3, pH 7, and pH 11 with 0.6M concentration of NaCl for 5 hours was represented as bar diagram in the Figure 8. It was found that, the corrosion rates obtained from the salt spray testing was much higher than the rates obtained from the potentiodynamic polarization tests. It was due to spraying effect where recycling of the solution could not take into account, while in potentiodynamic polarization test, there is a substantial increase in the pH of the solution during its exposure causing alkalization or basification of the solution with the increase of reactivity and time. However, both the corrosion tests causing pits to grow. On the other hand, exposure conditions of potentiodynamic polarization test prevails the continuous presence of water, resulted in the removal of corrosion by-products and the removal of surrounding magnesium, meaning that the pit area would decreased in the exposed surface of the specimen during polarization test. First, the removal of the corrosion products on the exposed surface of polarization test would reduce the ability of the pits to continue growing, as the corrosion products trap chloride ions within the pits. In the salt spray environment, where the salt water is not present continuously, the corrosion products can build up, trapping chloride ions, and allowing the pits to grow even when there is no water present. Second, the removal of the surrounding magnesium is caused by the presence of water, meaning that the continuous presence of water would remove magnesium and prevent pit growth. In this case of the salt spray environment, water is only present in the drying phase, any general corrosion is stopped. With general corrosion stopped and the corrosion products left in place, the pits on the salt spray surfaces are able to grow unabated. Therefore, the corrosion rate was higher in salt spray environment than the corrosion rate obtained from polarization test.

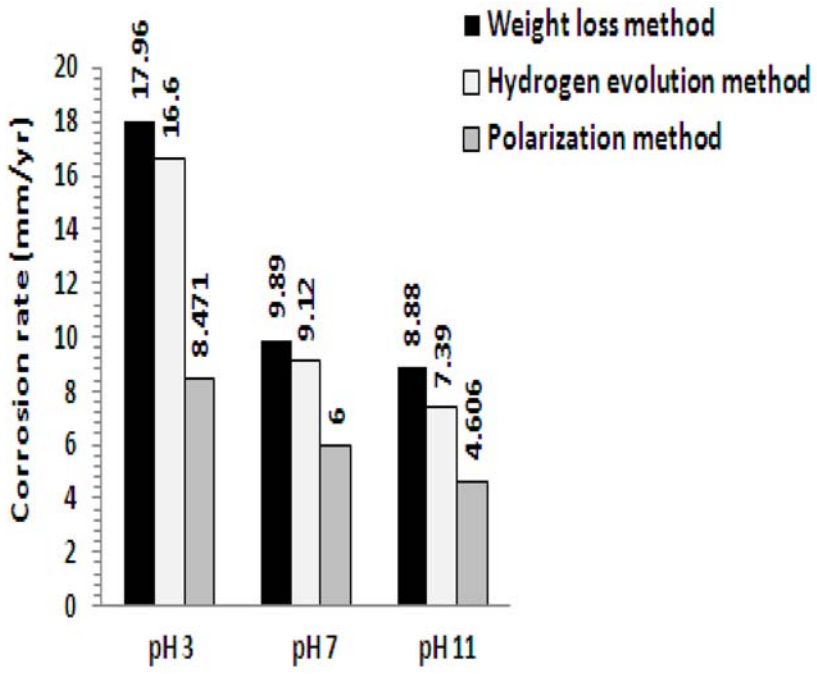

Figure 8. Comparative estimation of corrosion rate of specimen with different pH values of pH 3, pH 7, and pH 11 with 0.6M concentration of NaCl for 5 hours.

Figure 9 shows the effect of pH on pit morphology of the corroded specimen exposed in 0.6M concentration of NaCl for 5 hours with different pH values of pH 3, pH 7, and pH 11 for both salt spray test and potentiodynamic polarization test. During salt spray testing, the density of the pit formed in exposing lower pH (acidic) solution is quite high, comparing with the neutral and alkaline solution. It was observed that, the matrix shows the pitting marks and the pitting corrosion that has taken place at the friction stir welded microstructure. The particles are Mn-Al compound and fragmented $Mg_{17}Al_{12}$. The numbers of pits were more in the joints when it is sprayed with the solution of low pH. Hence, the corrosion rate increases with the decrease in pH value. Since, the increase of grain and grain boundary in the joints, the grain boundary acts cathodic to grain causing micro galvanic effect. The presence of

micro-galvanic effect between the α-phase and the β-phase formed due to the presence of aluminum. During polarization test, the grain boundaries of the specimen get attacked and its gravity varies with the parameters used in the experiment. Corrosion tends to be concentrated in the area adjacent to the grain boundary until eventually the grain may be undercut and fall out [22].

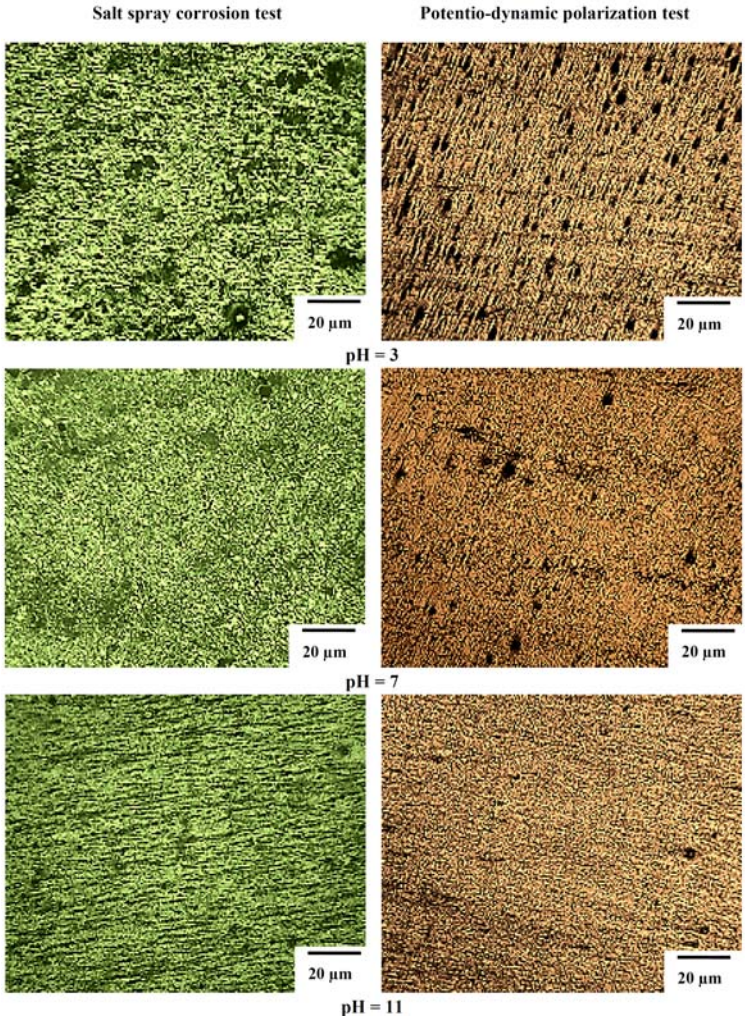

Figure 9. Effect of pH value on pit morphology with different pH values of pH 3, pH 7, and pH 11 with 0.6M concentration of NaCl for 5 hours.

4.2. Effect of chloride ion concentration on corrosion rate

Figure 10 shows the effect of chloride ion concentration on Tafel plots exposed in pH 7 for 5 hours with different chloride ion concentration of 0.2M, 0.6M, and 1M. It was observed that with the increase of chloride ion concentration of the solutions, the anodic curve of the materials showed a shift to higher current density values. And corrosion potential shifted to more negative (active) values with the increase in chloride ion concentration, which may explain by the adsorption of chloride ion on the alloy surface at weak parts of oxide film. Thus, the increase in corrosion rate with the increasing chloride ion concentration attributed the participation chloride ions in the dissolution reaction. It was considered that the corrosion becomes severe owing to the penetration of hydroxide film by Cl^-ion. This corrosion behaviour was consistent with the current understanding that the corrosion behaviour of magnesium alloys was governed by a partially protective surface film with the corrosion reaction occurring predominantly at the breaks or imperfections of the partially protective film.

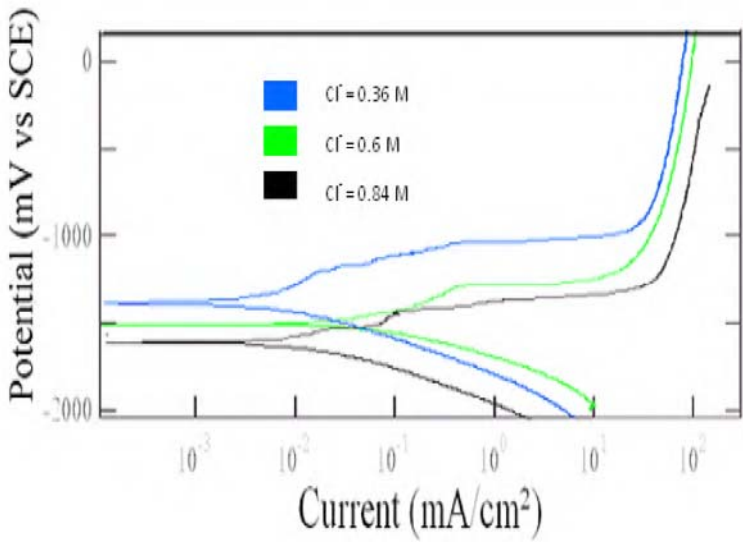

Figure 10. Effect of chloride ion concentration on Tafel plots exposed in pH 7 for 5 hours with different chloride ion concentration of 0.2M, 0.6M, and 1M.

Figure 11 represents the comparison chart for the corrosion rate of specimen exposed in pH 7 for 5 hours with different chloride ion concentration of 0.2M, 0.6M, and 1M obtained from both the corrosion tests. This is consistent with the detailing of the protective layer. With the increase of chloride ion concentration, the protective layer $Mg(OH)_2$ changed into soluble $MgCl_2$ layer for salt spray corrosion and $Mg(OH)_2Cl_2$ for electrochemical corrosion. The corrosion rate was quite higher in salt spray corrosion test than the polarization test. It states that, the $MgCl_2$ was highly soluble compared to $Mg(OH)Cl_2$. Hence, the attack was much higher in salt spray corrosion test.

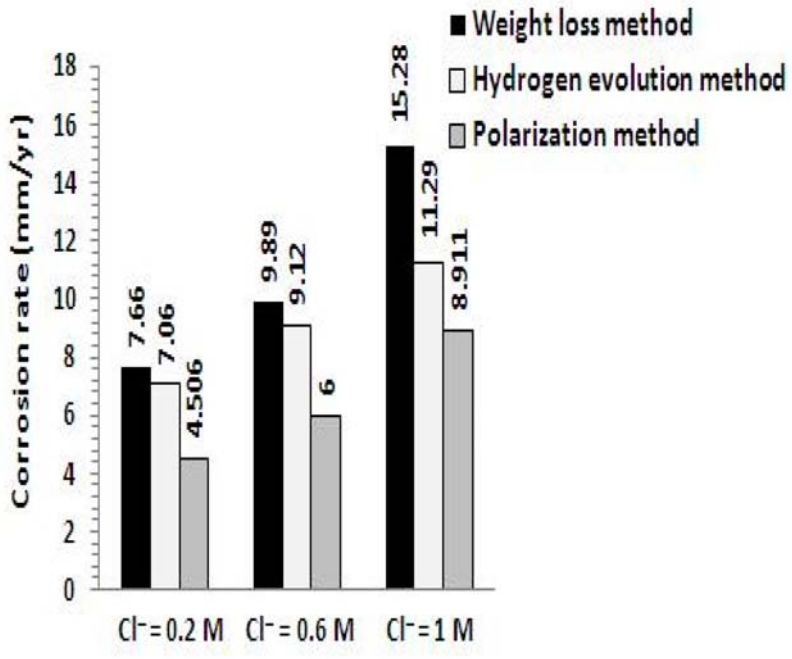

Figure 11. Comparative estimation of corrosion rate of specimen exposed in pH 7 for 5 hours with different chloride ion concentration of 0.2M, 0.6M and 1M.

Figure 12 shows the effect of chloride ion concentration on pit morphology of the corroded specimen exposed in pH 7 for 5 hours with different chloride ion concentration of 0.2M, 0.6M, and 1M for both salt

spray test and potentiodynamic polarization tests. During salt spray testing, it showed that the alloy exhibited a rise in corrosion rate with the increase in Cl^- concentration and thus the change of Cl^- concentration affected the corrosion rate much more in higher concentration solutions than that in lower concentration solutions. When more Cl^- in NaCl solution promoted the corrosion, the corrosive intermediate (Cl^-) would be rapidly transferred through the outer layer and reached the substrate of the alloy surface. Hence, the corrosion rate was increased [22]. While in polarization tests, the specimen exhibited a rise in corrosion rate with increase in Cl^- concentration and thus the change of Cl^- concentration affected the corrosion rate much more in higher concentration solutions than that in lower concentration solutions.

Chloride ions were aggressive for magnesium. The adsorption of chloride ions to oxide covered magnesium surface transformed $Mg(OH)_2$ to easily soluble $MgCl_2$. It was considered that the corrosion becomes severe owing to the penetration of hydroxide film by Cl^- ion and thereby the formation metal hydroxyl chloride complex, which governed the following reaction:

$$Mg^{2+} + 2H_2O + 2Cl^- \longrightarrow 2Mg(OH)_2Cl_2. \quad (11)$$

Concerning about the pit characteristics, more number of pits were observed in the specimen exposed to polarization test. This can be explained by the exposure environment. The salt spray was cyclical, chloride ions were only exposed to the surface of brief time, which would reduce how often new pits could form. The exposed surfaces during polarization test were continuously exposed to dissolved chloride ions, meaning new pits could form at any point. The ability of the pits to form whenever desired on the polarized surfaces means that depth would not be affected. However, because pits could only form during chloride ion exposure period on the salt spray surfaces, the time separating the exposure would be a major determining force in pit depth.

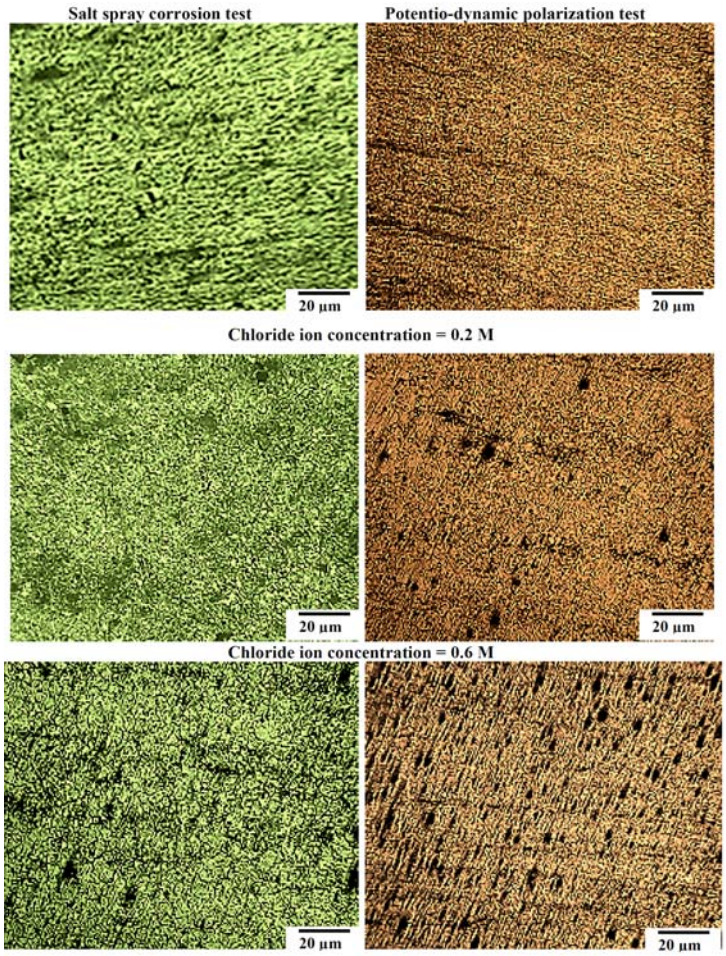

Figure 12. Effect of chloride ion concentration on pit morphology exposed in pH 7 for 5 hours with different chloride ion concentration of 0.2M, 0.6M, and 1M.

4.3. Effect of corrosion time on corrosion rate

Figure 13 shows the effect of exposure time on the Tafel plots of the specimen exposed in pH 7 with chloride ion concentration of 0.6M NaCl exposed 1h, 5h, and 9h. The corrosion potential shifted to a more positive direction with the increase in exposure time, the anodic branches are shifted to the more positive potential direction compared, indicating the

anodic dissolution is retarded with the increase of exposure time. As a result, the corrosion current also decreases with increasing exposure time. It was suggested that the existence of the corrosion film of NaCl solution with the increase of exposure time. In the early stages of the corrosion process, the anodic dissolution of AZ61A weldments is balanced by hydrogen evolution in the cathodic areas in NaCl solution. These corrosion products which in turn depressed the corrosion rate due to the passivation in the medium [11]. It results that there was an increase in hydrogen evolution with the increasing exposure time, which tends to increase the concentration of OH^- ions strengthening the surface from corrosion causing further. Since the strength of the electrolyte reduces from acidity to the alkalinity with the increases of time.

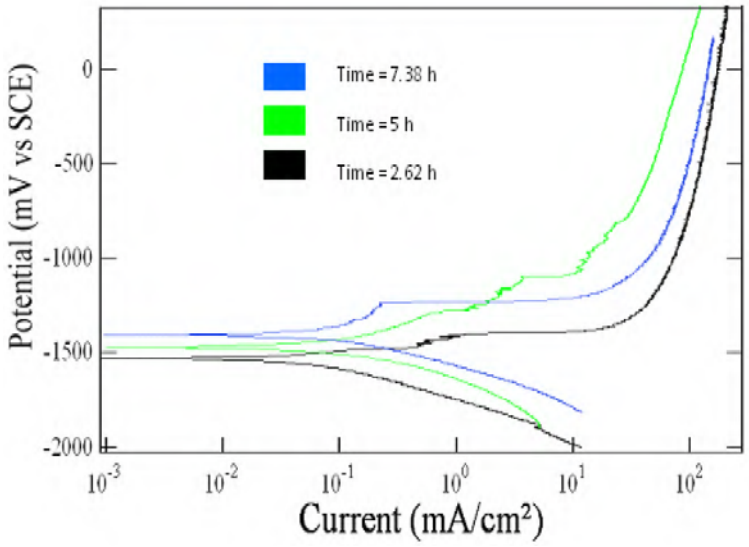

Figure 13. Effect of exposure time on Tafel plots of the specimen exposed in pH 7 with chloride ion concentration of 0.6M NaCl exposed 1h, 5h, and 9h.

This is attributed to corrosion occurring over increasing fraction of the surface was observed, which is the insoluble corrosion products [30]. The insoluble corrosion products on the surface of the alloy could slow down the corrosion rate.

$$Mg \longrightarrow Mg^{2+} + 2e^{-}. \quad (12)$$

$$2H_2O + 2e^{-} \longrightarrow 2OH^{-} + H_2. \quad (13)$$

$$Mg^{2+} + 2OH^{-} \longrightarrow Mg(OH)_2. \quad (14)$$

Figure 14 shows the comparison of the corrosion rate obtained during the salt spray and polarization test of the specimen exposed in pH 7 with chloride ion concentration of 0.6M NaCl exposed 1h, 5h, and 9h. With the increase of corrosion time, the corrosion rate decreases for both the specimens. It proved that the protective layer made a predominant role to strike against corrosion with the increment of time. The corrosion rate seems higher in salt spray corrosion test due to the spraying effect, while in exposed condition, the protective layer formed during polarization test was enhanced by the alkalization of the solution.

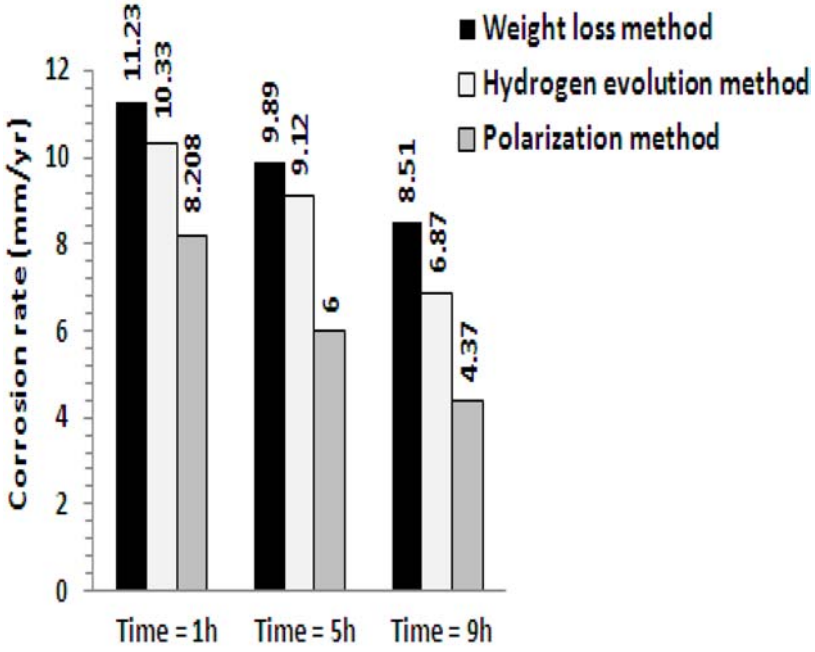

Figure 14. Comparative estimation of corrosion rate of the specimen exposed in pH 7 with chloride ion concentration of 0.6M NaCl exposed 1h, 5h, and 9h.

Figure 15 shows the effect of corrosion time on pit morphology of the corroded specimen exposed in pH 7 with chloride ion concentration of 0.6M NaCl exposed 1h, 5h, and 9h for both salt spray testing and potentiodynamic polarization test. The mode of microstructural features was comparatively same during corrosion testing for both the tests as its corrosion time taken into an account. The FS welded specimens possess refined grain and quite a lot of β particles were distributed continually along the grain boundary. In this case, β phase particles cannot be easily destroyed and, with the increase of corrosion time, the quantity of β phases in the exposed surface would increase and finally play the role of corrosion barrier [23]. Although, there are some grains of α phase still being corroded, most of the remaining α phase grains are protected under the β phase barrier, so the corrosion rate decreased with the increase in corrosion time. Thus, the corrosion morphology of the alloy was predominantly controlled by the β phase distribution [30]. As seeing the pit number density, both the tested specimen begins decline in its count of the pits. The distance between the pits were increased, meaning that, the pit area was highly protected with the magnesium hydroxide layer, and also, uninhibited by general corrosion removing magnesium surrounding the pit.

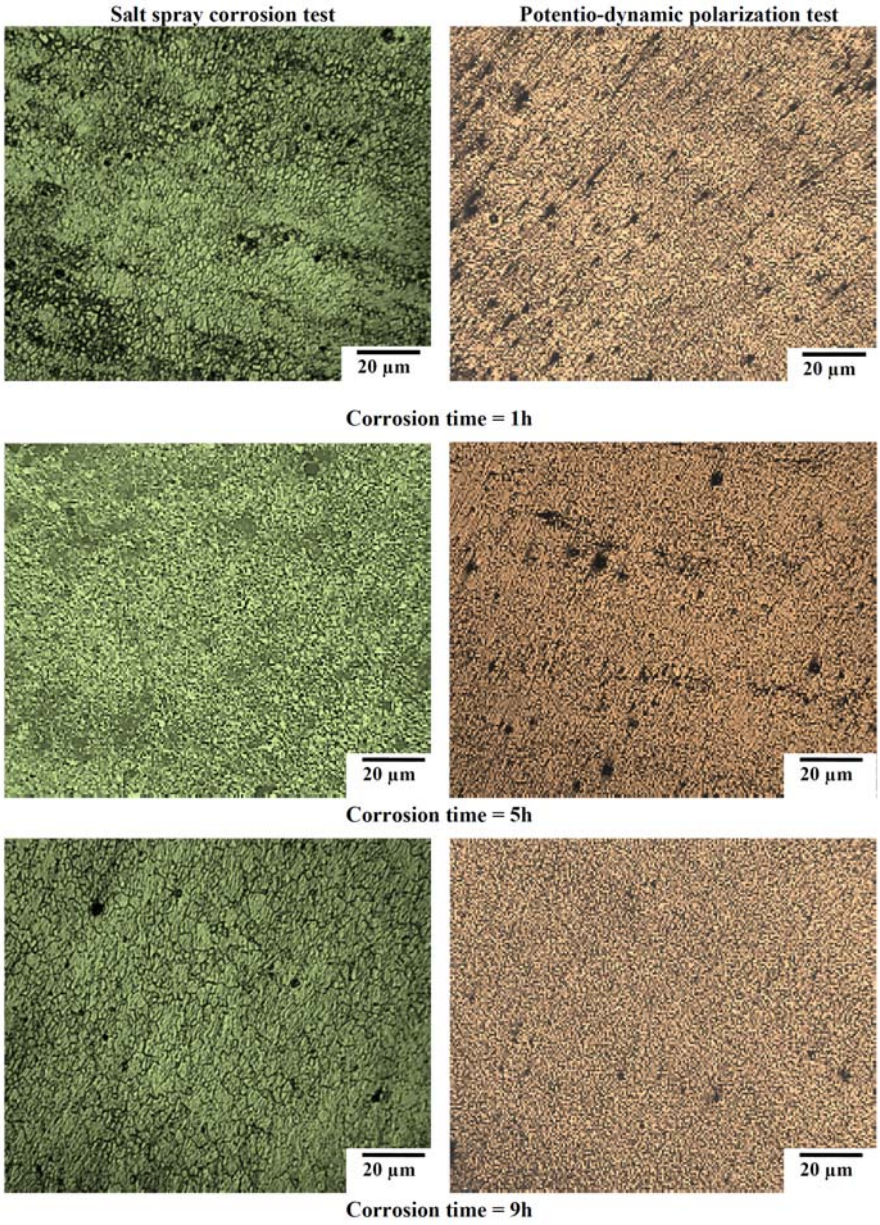

Figure 15. Effect of corrosion time on pit morphology of the specimens exposed in pH 7 with chloride ion concentration of 0.6M NaCl exposed 1h, 5h, and 9h.

4.4. Scanning electron microscopy

Figure 16 shows the SEM - EDAX of the specimen underwent salt spray corrosion test at different spraying time (a) 1 hour and (b) 9 hours with pH 7 and chloride ion concentration 0.6M. The corrosion products comprise of the hydroxide layer. Since, with the increase in immersion time, the hydroxide layer formed is the dominant factor to avoid further corrosion. This is attributed by the presence of Mg and O from EDAX, results that the corrosion products mainly composed of oxygenated protective layers. The oxygenated peaks shows higher intensity with the specimen sprayed for 9 hours. This means with the increase of spraying time, enhances the protective layer to constraint the further corrosion. The corrosion was occurring over an increasing fraction of the surface was observed, which is the insoluble corrosion products $Mg(OH)_2$. Thus, the corrosion rate decreases with the increase of exposure time. It was noted that from the microstructure of friction stir welded stir zone before tests the grain was refined and quite lots of β particles distribute continually along the grain boundary. During corrosion testing, β phase particles cannot be easily destroyed and, with the increase of corrosion time, the quantity of β phases in the exposed surface will increase and finally play the role of corrosion barrier. Although, there were some grains of α phase still being corroded, most of the remaining α phase grains were protected under the β phase barrier, so the corrosion attack was decreased with the increase of spraying time.

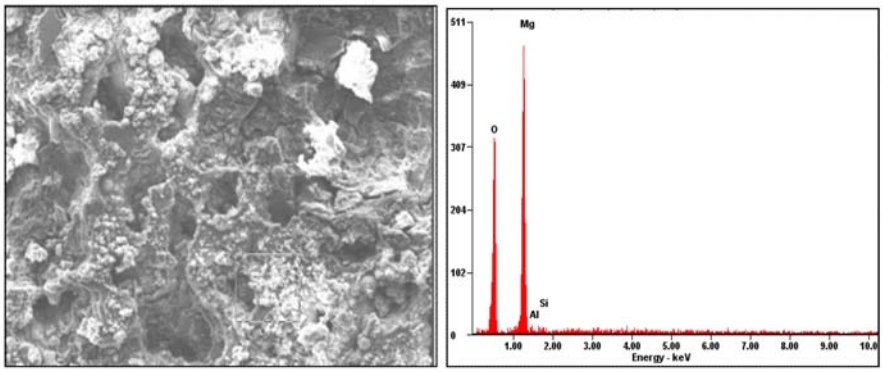

(a) Spraying time = 1 hour

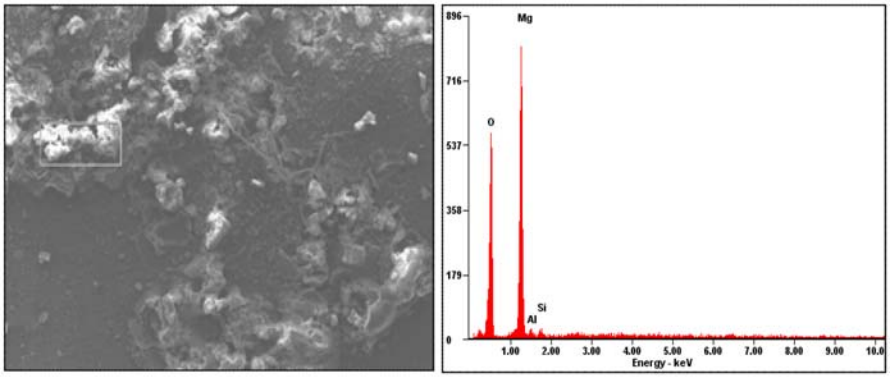

(b) Spraying time = 9 hours

Figure 16. Scanning electron micrograph with EDAX of corrosion test specimens underwent salt spray corrosion test at different spraying time (a) 1 hour and (b) 9 hours with pH 7 and chloride ion concentration 0.6M.

Figure 17 shows the SEM-EDAX results for the specimen underwent potentiodynamic polarization test at different exposure time (a) 1 hour and (b) 9 hours with pH 7 and chloride ion concentration 0.6M, that the corrosion products containing Mg and O in the presence of NaCl. It has certain peaks of Cl^-, which indicates the corrosion products having the surface of the specimen shows more cracks over the corrosion products, where the Cl^- penetrate into the surface. When more Cl^- in NaCl solution promoted the corrosion, the corrosive intermediate (Cl^-) would be rapidly transferred through the outer layer and reached the substrate of the alloy surface [4]. The exposed surfaces during polarization test

were continuously exposed to dissolved chloride ions, meaning new pits could form at any point. The ability of the pits to form whenever, desired on the sprayed surfaces means that depth would not be affected. However, because pits could only form during chloride ion exposure period on the salt spray surfaces, the time separating the exposure would be a major determining force in pit depth. It was observed that, with the increase of corrosion time, the intensity of the chloride peaks was starting diminished; it seems, with the increase of corrosion time, the magnesium hydroxide layer dominates the corrosion process to avoid further attack [8].

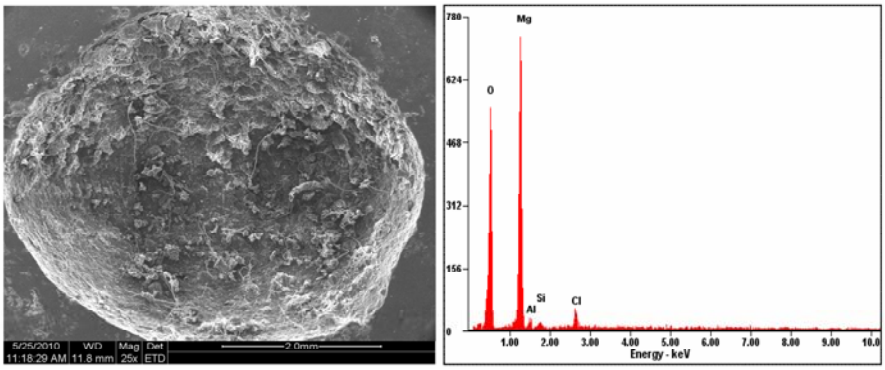

(a) Exposure time = 1 hour

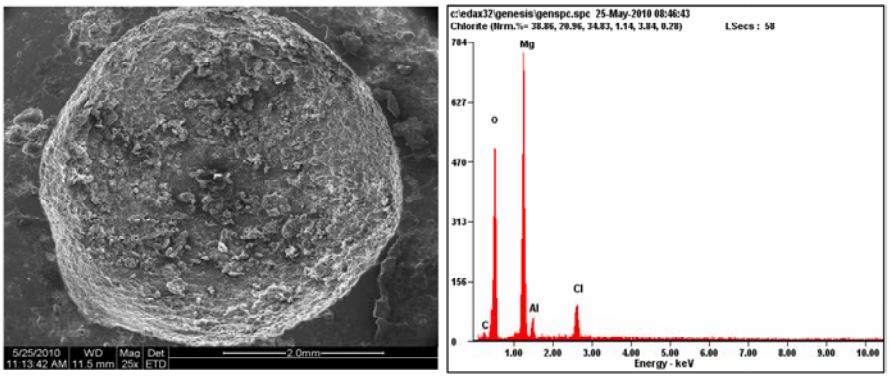

(a) Exposure time = 9 hours

Figure 17. Scanning electron micrograph with EDAX of corrosion test specimens underwent potentiodynamic polarization test at different exposure time (a) 1 hour and (b) 9 hours with pH 7 and chloride ion concentration 0.6M.

4.5. X-Ray diffraction analysis

Figure 18(a) shows the XRD pattern to predict the composition of corrosion products and phase in the specimen subjected to salt spray corrosion tests with spraying time 9 hours. There detect number of peaks relates to the β phase ($Mg_{17}Al_{12}$). Since the increase of grain and grain boundary in the weld metal region, the grains boundary acts cathodic to grains causing micro galvanic effect. This was defined earlier that, the β phase found the stir zone was not continuous, which thereby enhances to cause micro-galvanic coupling. The corrosion tends to be concentrated in the areas adjacent to the grain boundary until eventually the grain may be undercut and fall out. However, higher peaks of $Mg(OH)_2$ phases are detected in the Figure 18(b) exposed for 9 hours. During potentiodynamic polarization test, the $Mg(OH)_2$ is the dominant product in the corrosion zone with the increment of exposure time. $Mg(OH)_2$ (brucite) has a hexagonal crystal structure and undergoes easily basal cleavage causing cracking and curling in the film, which could play a major role in reducing the corrosion behaviour and the corrosion rate [9, 25].

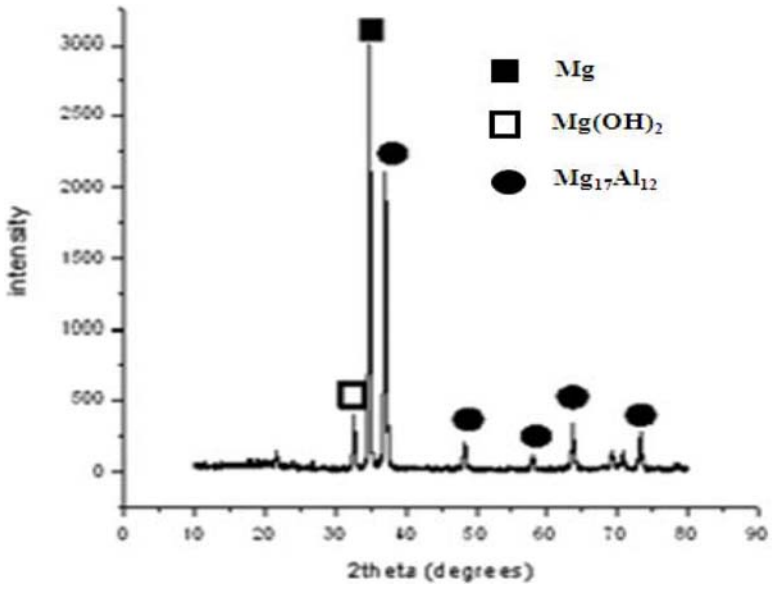

(a)

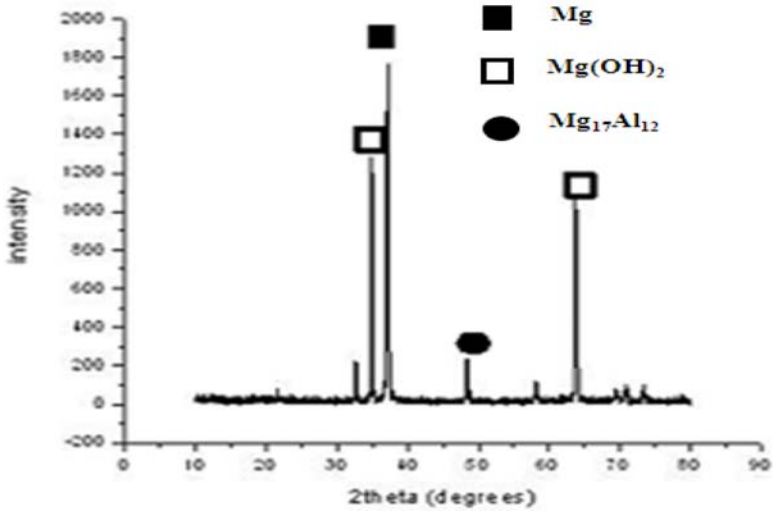

(b)

Figure 18. XRD pattern of corrosion test specimens underwent (a) salt spray corrosion test and (b) potentiodynamic polarization test with corrosion time 9 hours.

5. Conclusions

Friction stir welded AZ61A magnesium alloy welds was studied to understand its corrosion rates under two different environments: salt fog and electrochemical environments. The stir zones were examined at various corrosion parameters to determine the effect of two environments experienced for service applications. The results observed were:

(1) The corrosion rate obtained from the hydrogen evolution rate was agrees with the corrosion rate obtained from the weight loss method. This proved that the hydrogen evolution was interrelated with the weight loss during corrosion.

(2) The corrosion rate was higher in salt fog environment than the electrochemical polarized environments. This is due to the fact; there is a substantial increase in the pH during potentiodynamic polarization test as the specimen exposed throughout the test. But, in salt spray test, the electrolyte was freshly used and not recycled. Therefore, it eliminates the basification in the solution to enhance the protection from corrosion.

(3) It results an increase in hydrogen evolution with the increasing corrosion time, which tended to increase the concentration of OH^- ions thereby increasing fraction of the surface was observed, which is the insoluble corrosion products $Mg(OH)_2$. The insoluble corrosion products on the surface of the alloy could slow down the corrosion rate for both the corrosion tests.

(4) The chloride ions are more aggressive to the magnesium alloys. Since increase in the chloride ion concentration enhance the corrosion behaviour. It was obvious from the observation of pit number densities, which increases with the increase in chloride ions.

(5) From this work, it was observed that, the AZ61A FSW joints were lower corrosion rate in the electrochemical environments than the salt fog environment. Thus, the FSW joints proved to give a long life from corrosion in electrochemical environments.

Acknowledgement

The authors would like to thank Centre for Materials Joining & Research (CEMAJOR), Department of Manufacturing Engineering, Annamalai University, Annamalai Nagar, for extending the facilities of Materials Joining Laboratory and Corrosion Testing Laboratory to carry out this investigation.

References

[1] Hikmet Altun and Sadri Sen, Studies on the influence of chloride ion concentration and pH on the corrosion of AZ63 magnesium alloy, Mater. Des. 25 (2004), 637-643.

[2] N. Aslan, Application of response surface methodology and central composite rotatable design for modelling and optimization of a multi gravity separator for chromite concentration, Powd. Tech. 185 (2008), 80-86.

[3] ASM International, Metals Handbook, Corrosion, 9th Edition, Vol. 13, ASM International, 1987.

[4] Robert Babion, Corrosion Tests and Standards: Application and Interpretation, ASTM International, 2005.

[5] G. E. P. Box and N. R. Draper, Empirical Model Building and Response Surface, John Wiley and Sons, New York, 1987.

[6] A. Dhanapal, S. Rajendra Boopathy and V. Balasubramanian, Developing an empirical relationship to predict the corrosion rate of friction stir welded AZ61A magnesium alloy under salt fog environment, Mater. Des. 32 (2011), 5066-5072.

[7] M. G. Fontana and N. D. Greene, Corrosion Engineering, McGraw-Hill, New York, 1984.

[8] Lili Gao, Chunhong Zhang, Milin Zhang, Xiaomel Huang and Nan Sheng, The corrosion of a novel Mg-11Li-3Al-0.5RE alloy in alkaline NaCl solution, J. All. and Comp. 468 (2009), 285-289.

[9] H. P. Godard, W. B. Lepson, M. R. Bothewell and R. L. Kane, The Corrosion of Light Metals, Wiley, New York, 1967.

[10] Kok-Hui Goh, Teik-Thye Lim and Peng-Cheong Chui, Evaluation of the effect of dosage, pH and contact time on high-dose phosphate inhibition for copper corrosion control using response surface methodology (RSM), Corr. Sci. 50 (2008), 918-927.

[11] Nobuyoshi Hara, Yasuhiro Kobayashi, Daisuke Kagaya and Noburu Akao, Formation and breakdown of surface films on magnesium and its alloys in aqueous solutions, Corr. Sci. 49 (2007), 166-175.

[12] D. A. Jones, Principles and Prevention of Corrosion, Prentice-Hall, Englewood Cliffs, NJ, 1992.

[13] Tonya S. King, Vernon M. Chinchilli and Josep L. Carrasco, A repeated measures concordance correlation coefficient, Stat. Med. 26 (2007), 3095-3113.

[14] Lin Li, A concordance correlation coefficient to evaluate reproducibility, Biomet. 45 (1989), 255-268.

[15] O. Lunder and A. S. Langseth, Measurement of Hydrogen evolution from corroding Mg, SINTEF Metallurgy Corrosion Center (Internal Report), Norway, 1992.

[16] B. L. Modike and T. Ebert, Magnesium-properties, applications and potential, Mater. Sci. Engg. A 302 (2001), 37-45.

[17] T. Nagasawa, M. Otsuka, T. Yokota and T. Ueki, Structure and Mechanical Properties of Friction Stir Weld Joints of Magnesium Alloy AZ31; in: H. I. Kaplan, J. Hryn and B. Clow [Eds.], Magnesium Technology 2000 TMS, Warrendale, (2000), 383-387.

[18] L. M. Peng, J. W. Chang, X. W. Guo, A. Atrens, W. J. Ding and Y. H. Peng, Influence of heat treatment and microstructure on the corrosion of magnesium alloy Mg-10Gd-3Y-0.4Zr, J. Appl. Electrochem 39 (2009), 913-920.

[19] Zhiming Shi, Ming Liu and Andrej Atrens, Measurement of the corrosion rate of magnesium alloys using Tafel extrapolation, Corr. Sci. 52 (2010), 579-588.

[20] G. L. Song and A. Atrens, Corrosion mechanisms of magnesium alloys, Adv. Eng. Mater. 1 (1999), 11-33.

[21] G. L. Song, A. Atrens and D. H. St. John, An hydrogen evolution method for the estimation of the corrosion rate of magnesium alloys, In: J. N. Hyrn (Ed.), Magnesium Technology 2001, New Orleans, USA, (2001), 255-262.

[22] G. L. Song, Recent progress in corrosion and protection of magnesium alloys, Adv. Eng. Mater. 7 (2005), 563-586.

[23] Yingwei Song, Dayong Shan, Rongshi Chen and En-Hou Han, Effect of second phases on the corrosion behaviour of wrought Mg-Zn-Y-Zr alloy, Corr. Sci. 52 (2010), 1830-1837.

[24] H. H. Uhlig, Corrosion and Corrosion Control, Wiley, New York, 1973.

[25] Lei Wang, Bo-Ping Zhang and Tadashi Shinohara, Corrosion behaviour of AZ91magnesium alloy in dilute NaCl solutions. Mater. Des. 31 (2010), 857-863.

[26] D. Weiss et al., Corrosion Resistance Evaluation of Magnesium and Magnesium Alloys by an Ion Selective Electrode, Proceedings of the First Israeli International Conference on Magnesium Science and Technology, 1997.

[27] Weifeng Xu, Jinhe Liu and Hongqiang Zhu, Pitting corrosion of friction stir welded aluminum alloy thick plate in alkaline chloride solution, Electrochimica Acta 55 (2010), 2918-2923.

[28] R. C. Zeng, J. Zhang, W. J. Huang, W. Dietzel, K. U. Kainer, C. Blawert and W. Ke, Review of studies on corrosion of magnesium alloys, Trans. Non-Ferr. Met. Soc. China 16 (2006), s763-s771.

[29] R. C. Zeng, W. Dietzel, R. Zettler, J. Chen and K. U. Kainer, Microstructure evolution and tensile properties of friction-stir-welded AM50 magnesium alloy, Trans. Non-Ferr. Met. Soc. China 18 (2008), s76-s80.

[30] Zhimin Zhang, Hongyan Xu and Baocheng Li, Corrosion properties of plastically deformed AZ80 magnesium alloy, Trans. Non-Ferr. Met. Soc. China 20 (2010), s697-s702.

[31] Ming Zhao, Shusen Wu, Ji-Rong Luo, Y. Fukuda and H. Nakae, A Chromium-free conversion coating of magnesium alloy by a phosphate-permanganate solution, Surf. Coat. Tech. 200 (2006), 5407-5412.

[32] M. C. Zhao, M. Liu, G. L. Song and A. Atrens, Influence of microstructure on corrosion of As-cast ZE41, Adv. Eng. Mater. 10 (2008), 104-111.

[33] M. C. Zhao, M. Liu, G. L. Song and A. Atrens, Influence of the beta-phase morphology on the corrosion of the Mg alloy AZ91, Corr. Sci. 50 (2008), 1939-1953.

[34] M. C. Zhao, M. Liu, G. L. Song and A. Atrens, Influence of the pH and chloride ion concentration on the corrosion of Mg alloy ZE41, Corr. Sci. 50 (2008), 3168-3178.

[35] M. C. Zhao, P. Schmutz, S. Brunner, M. Liu, G. L. Song and A. Atrens, An exploratory study of the corrosion of Mg alloys during interrupted salt spray testing, Corr. Sci. 51 (2009), 1277-1292.

■